Mechanical Systems and Signal Processing 222 (2025) 111762

Contents lists available at ScienceDirect

Mechanical Systems and Signal Processing

journal homepage: www.elsevier.com/locate/ymssp

Total harmonic distortion estimation in piezoelectric micro-electro-mechanical-system loudspeakers via a FEM-assisted reduced-order-model

Chiara Gazzola, Alberto Corigliano, Valentina Zega *

Department of Civil and Environmental Engineering, Politecnico di Milano, Milano, Italy

ARTICLE INFO

Communicated by X. Jing

Keywords:
MEMS loudspeaker
Reduced Order Model (ROM)
Sound Pressure Level (SPL)
Total Harmonic Distortion (THD)
Piezoelectric material
Equivalent circuit

ABSTRACT

Piezoelectric micro-electro-mechanical-system (MEMS) loudspeakers are attracting growing research interest in the last years due to the increasing interest towards miniaturization required by new wireless audio devices. Finite Element Models (FEM) and Lumped Element Models (LEM) able to accurately simulate their linear response have been recently proposed in the literature. However, a nonlinear model suitable to predict the Total Harmonic Distortion (THD) of these devices is to date still missing. In this work, we present a FEM-assisted lumped-parameters equivalent circuit for THD estimation which accounts for geometric nonlinearities and piezoelectric hysteresis. The loudspeaker nonlinear electro-mechanical domain is simulated through a Reduced Order Model (ROM) which considers as basis function the pre-stressed undamped actuated mode of the device computed via FEM, to account for loudspeaker diaphragms of arbitrarily complex geometry. Parameters of the acoustical circuit are computed through analytical formulas. The good matching between numerical predictions and experimental results, carried out on a piezoelectric MEMS loudspeaker prototype for in-ear condition, demonstrates the accuracy of the proposed tool.

1. Introduction

Loudspeakers are multiphysics transducers able to convert an electrical signal to a corresponding sound pressure by typically exploiting the mechanical deformation of a physical diaphragm.

The increased global demand for miniaturization of portable audio devices without impairing performances such as sound quality or battery life, is making MEMS microspeakers an attracting research topic [1–4] thanks to their intrinsic small dimensions, on-chip integrability and cost-efficiency in mass production. Traditional microspeakers based on electrodynamic or balanced armature schemes offer instead limited incremental improvements towards the market requirements for modern devices to become smaller and lighter.

In the last years, several MEMS speakers have been proposed for free-field [5–8] and in-ear applications [9–13]. The most promising solutions are relative to the latter configuration, being the deflections of the mechanical diaphragm required to reach a target Sound Pressure Level (SPL) order of magnitude smaller with respect to the free-field case.

Among the different possible actuating principles exploitable in MEMS speakers, the piezoelectric one has been recognized as the most promising due to the relatively high driving force achievable at low actuation voltages [5,11–15].

* Corresponding author.
E-mail address: valentina.zega@polimi.it (V. Zega).

https://doi.org/10.1016/j.ymssp.2024.111762
Received 4 March 2024; Received in revised form 29 May 2024; Accepted 20 July 2024
Available online 31 July 2024

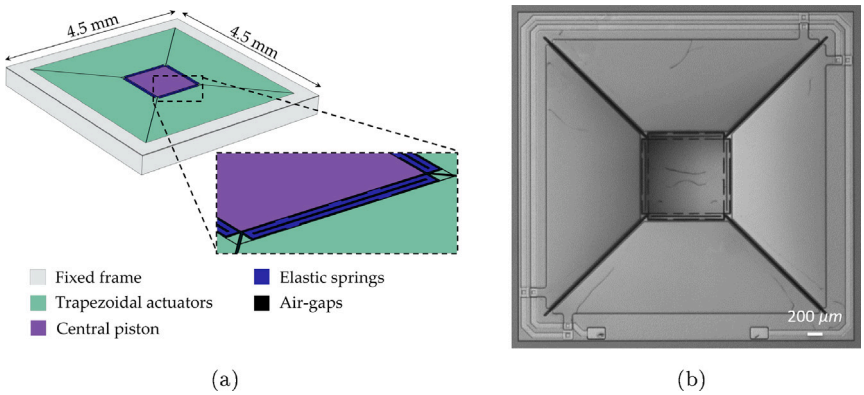

Fig. 1. (a) Schematic view of the reference piezoelectric MEMS loudspeaker, together with a close-up view of the folded springs (in blue) connecting the trapezoidal plates hosting the PZT material (in green) with the central piston (in violet) (b) SEM image of the fabricated device.

Multiphysics Finite Element Models (FEM) have been recently proposed to accurately predict the linear response of piezoelectric MEMS loudspeakers [16]. They usually result in high computational costs that cannot be afforded if real-time design optimization must be performed. On the other side, Lumped Element Models (LEM) [17] rely on the representation of spatially distributed physical systems through a set of lumped elements and are emerging as a powerful tool for a fast prediction of MEMS loudspeakers responses [5,18,19]. LEM are suitable for MEMS loudspeakers modelling for a twofold reason. Firstly, the underlying hypothesis, that the device's length scale is much smaller than the wavelength of the governing physical phenomenon, is fully satisfied across nearly the entire audible frequency range. Secondly, the mechanical diaphragm of MEMS loudspeakers is often designed to behave as a single-degree-of-freedom oscillator [5,11,12,16,20–22]. Combined lumped parameter and reduced-order finite element modelling have been also recently proposed to estimate sound radiation from multiple speakers [23].

In this work, we want to make a step further in terms of piezoelectric microspeakers modelling. Our goal is to predict not only the linear response, but also the Total Harmonic Distortion (THD) of a typical piezoelectric MEMS speaker. The THD is the indicator usually adopted to evaluate the linearity of a loudspeaker, being defined as the ratio between the sum of the effective values of the sound pressure higher harmonic components and the effective value of the first harmonic. Several sources of nonlinearities can cause distortion in a loudspeaker output pressure, coming both from the signal processing (e.g. amplifier saturation, transistor nonlinearities) and the transduction. The latter is usually more relevant and can be ascribed to the speaker mechanical structure (mechanical nonlinearities of the moving diaphragm) and to the nonlinearities of the transduction principle, like piezoelectric hysteresis or magnetic saturation in electromagnetic drivers [24].

Predicting Total Harmonic Distortion (THD) is crucial for enhancing sound fidelity in piezoelectric microspeakers, especially given the unavoidable nonlinear effects. However, a comprehensive nonlinear model for these devices is still lacking.

Different techniques, *e.g.* state space models, port-Hamiltonian systems, Hammerstein models and power series, have been indeed proposed so far to model the nonlinearities of classical macroscale [24–35] and microscale [36–42] electrodynamic speakers, but only very recently, nonlinear models able to predict the THD of MEMS speakers appeared in the literature for the first time. In 2022, for instance, Monsalve et al. [27] proposed a large-signal equivalent circuit to model the THD of asymmetric electrostatic transducers and compared the results of the proposed lumped model with the numerical and experimental data published by [43]. To the Authors' best knowledge, the first and only work related to the THD prediction of piezoelectric microspeakers appeared in 2021. In [44], it was proposed a state-space model able to account for the nonlinear mechanical stiffness, transduction coefficient and capacitance of a cantilever-based PZT loudspeaker. The piezoelectric hysteresis was however not included in the model and this lead to a quite significant underestimation of the THD [45].

In this work, we propose a FEM assisted nonlinear LEM accounting for geometric nonlinearities and piezoelectric hysteresis and we demonstrate a good agreement between predictions and experimental results obtained on the device previously published in [9].

The paper is organized as follows: the reference piezoelectric microspeaker design exploited to validate the proposed procedure is presented in Section 2, the electro-mechano-acoustic nonlinear model is detailed in Section 3, while numerical results are reported in Section 4 and compared with experiments in Section 5. Finally, in Section 6, conclusions are drawn together with future perspectives.

2. Reference loudspeaker

The MEMS loudspeaker recently proposed in Gazzola et al. [9] is here employed as reference structure. A schematic view and a Scanning Electron Microscope (SEM) image of the device are reported in Figs. 1(a) and 1(b), respectively. The moving mechanical structure of the proposed device is composed by four trapezoidal actuators connected to a central squared piston through properly sized folded elastic springs and it is anchored to the substrate through an external silicon frame. Ten μm-width air-gaps separate the different mechanical components. The total footprint of the device, comprising the 350 μm wide external frame, is 4.5×4.5 mm^2. The first electro-mechanical vibration mode occurs at 10.9 kHz.

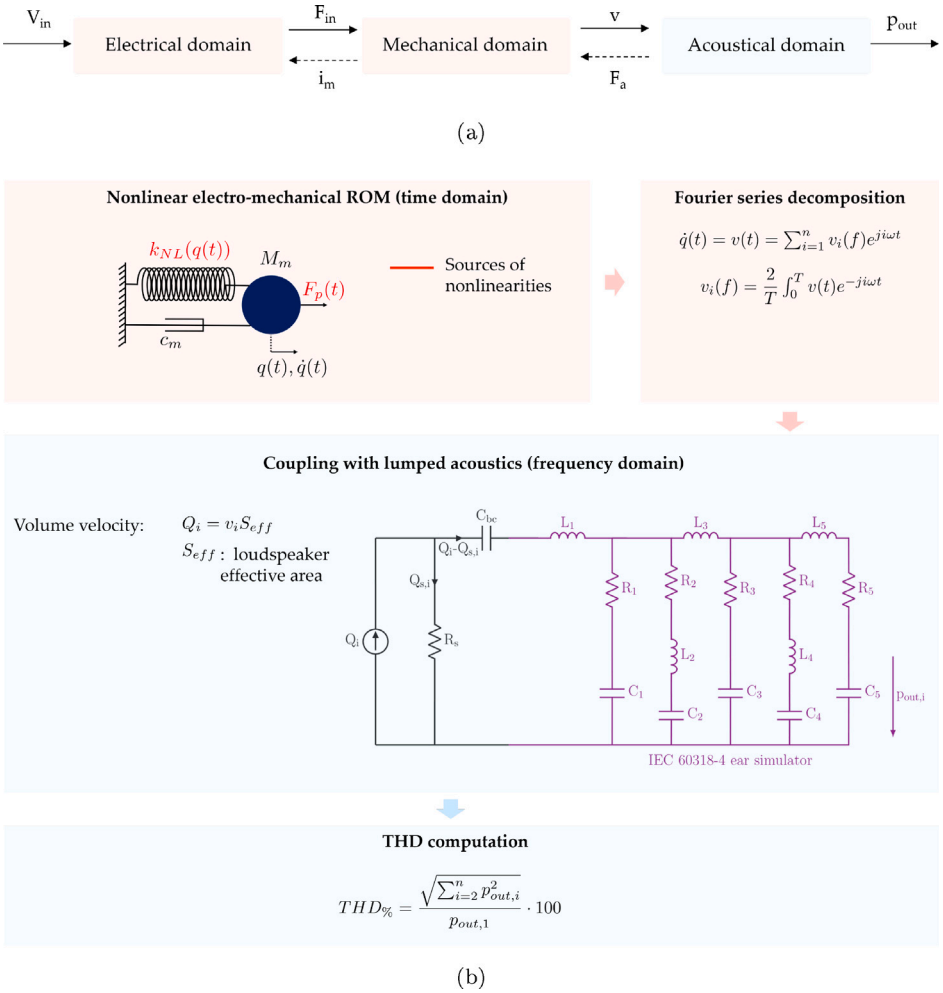

Fig. 2. (a) General block diagram representing the different physical domains involved in the functioning of a loudspeaker. (b) Flowchart illustrating the proposed procedure for the modelling of the nonlinear response of piezoelectric MEMS loudspeaker. The nonlinear electro-mechanical domain is reduced to a one-degree-of-freedom system, solved in time domain. The time dependent loudspeaker velocity is decomposed in Fourier series retaining n harmonic components. The latter, upon multiplication by the speaker effective area, are used as coupling variables to the n linear equivalent circuits representing the acoustic domain for in-ear condition (the IEC 60318-4 ear simulator is reported in violet). The THD is then computed from the n output pressures at the ear simulator microphone, obtained at the poles of the capacitor C_5.

3. Nonlinear model

The general block diagram representing the different physical domains involved in the functioning of a piezoelectric loudspeaker is reported in Fig. 2(a). The input electrical signal V_{in} is transformed into the output sound pressure p_{out} through two energy transformations: from electrical domain to mechanical domain and from mechanical domain to acoustical domain. In particular, the input electrical signal V_{in} is converted into a mechanical force F_{in} through the selected transduction mechanism, *i.e.* piezoelectricity, and the force F_{in} is converted into the velocity v of the mechanical component via the mechanical impedance, representing the frequency dependent response of the mechanical oscillator. Mechanical vibrations finally induce a perturbation of the surrounding air with a consequent generation of sound pressure.

The fundamental hypotheses assumed in the proposed model is that of one-way coupling between the electrical domain and the mechanical domain and between the mechanical domain and the acoustic domain, *i.e.* the electrical current induced by the direct piezoelectric effect (i_m in Fig. 2(a)) and the acoustic load (F_a in Fig. 2(a)) are neglected. The first assumption have been proved to be accurate for thin-film piezoelectric actuators [19,46–49] for which the one-way piezoelectric constitutive law can be employed. The effect of the acoustic load on the loudspeaker velocity will be discussed in Section 4.

Fig. 2(b) describes the main steps of the THD model here proposed. The basic idea is that the electro-mechanical domain, which contains the main sources of nonlinearities, is solved in time domain, while the acoustic domain is considered as linear and works

in the frequency domain. More in details, the electro-mechanical domain is simulated through a Reduced Order Model (ROM) which considers as basis function the pre-stressed undamped actuated mode of the device, solved in time in terms of loudspeaker displacement and velocity in the whole audible range. At each forcing frequency, the loudspeaker velocity is decomposed in Fourier series retaining n harmonic components that, upon multiplication by the speaker effective area, are used as coupling variables to the n linear equivalent circuits representing the acoustic domain for in-ear condition (the IEC 60318-4 ear simulator is reported in violet in Fig. 2(b)). The THD is finally computed from the n output pressures evaluated at the ear simulator microphone.

3.1. Electro-mechanical modelling

In this subsection, the equations governing the electro-mechanical problem are reported considering their strong and weak form fashion. How the dimensionality of the nonlinear model is reduced to a one-degree-of-freedom system is then explained. The resulting ROM is defined as FEM-assisted as its coefficients are numerically computed via FEM, to account for loudspeaker diaphragm of arbitrarily complex geometries.

3.1.1. Piezoelectric modelling

Ferroelectric materials, and in particular Lead Zirconate Titanate (PZT), thin films are largely employed in MEMS devices thanks to their high piezoelectric coefficients that allow to achieve relatively high actuation forces with a reduced footprint. The main feature of ferroelectric materials is the existence of a spontaneous polarization and the capability to re-orient it under an applied external electric field. Such property results in a polarization versus electric field hysteresis loop which is usually unwanted in MEMS devices because of its nonlinear nature. To limit such phenomenon, the piezoelectric actuation is often performed by adding an offset equal to half the input dynamics, thus avoiding the change of sign of the electric field. Despite such precaution, it has been demonstrated that ferroelectric materials hysteretical behaviour represents one of the major source of total harmonic distortion in PZT-actuated MEMS loudspeakers [9,44] and must be then carefully modelled.

A lot of research work has been already done in the literature to simulate the hysteretical behaviour of ferroelectric materials by exploiting different approaches and considering different scales of the problem [50–58]. In this contribution, the P2-formulation presented by Frangi et al. [46,47] for the nonlinear modelling of micro-mirrors actuated by piezoelectric thin-films is considered. It relies on a direct experimental measurement of the polarization field evolution and to the estimation of its effects on stresses and equilibrium resorting to some basic principles of the Landau–Devonshire theory of ferroelectric materials [54,59–61]. The choice to resort to a direct measurement of the polarization field is dictated by the wide variability of the hysteresis cycles of multi-grain sol–gel deposited thin films that can be hardly quantified and simulated [62], being strongly dependent on defects and small variations in the production technology. It is worth noting that the above formulation implicitly assumes an average uniform polarization of the thin film.

The polarization field $\boldsymbol{p}$ induces inelastic strains $\boldsymbol{E}^p$ such that the De Saint Venant–Kirchhoff constitutive law for large transformations and small strains reads:

$$\boldsymbol{S} = \mathcal{A} : (\boldsymbol{E} - \boldsymbol{E}^{\boldsymbol{P}}) + \boldsymbol{S_0} = \mathcal{A} : \boldsymbol{E}[\boldsymbol{u}] - \boldsymbol{S}^p[\boldsymbol{p}] + \boldsymbol{S_0}, \tag{1}$$

where $\boldsymbol{S}$ is the second Piola–Kirchhoff stress tensor, $\boldsymbol{S_0}$ are pre-stresses induced by the fabrication process, $\boldsymbol{E} = sym(\nabla \boldsymbol{u}) + \frac{1}{2}\nabla^T \boldsymbol{u} \cdot \nabla \boldsymbol{u}$ is the Green Lagrange strain tensor, being $\mathbf{u}$ the displacement field and ∇ the gradient operator. $\mathcal{A}$ is the fourth order elasticity tensor and $\boldsymbol{S}^p$ are the inelastic stresses induced by the polarization field $\boldsymbol{p}$.

According to the Landau–Devonshire theory of ferroelectric materials, inelastic strains induced by the polarization field can be expressed as:

$$\boldsymbol{E}^p = \mathcal{Q} : (\boldsymbol{p} \otimes \boldsymbol{p}), \tag{2}$$

being $\mathcal{Q}$ the fourth-order electrostrictive tensor.

The dynamic response of the system is defined by the conservation of linear momentum expressed with respect to the reference configuration Ω_0:

$$\rho_0 \ddot{\boldsymbol{u}} - \nabla \cdot \boldsymbol{P} = \mathbf{0}, \qquad \Omega_0 \times t \in (t_0, T_e] \tag{3}$$

being the right hand side null since body forces are here neglected. ρ_0 is the material density, $\boldsymbol{P}$ is the first Piola–Kirchhoff stress tensor and $\ddot{(\cdot)}$ is the second partial derivative with respect to time. All quantities are defined over the time span from t_0 to T_e. Boundary and initial conditions for Eq. (3) are:

$$\boldsymbol{P} \cdot \boldsymbol{n} = \mathbf{0} \quad \text{on } \partial\Omega_0^N \times t \in (t_0, T_e] \tag{4}$$

$$\boldsymbol{u} = \mathbf{0} \quad \text{on } \partial\Omega_0^D \times t \in (t_0, T_e] \tag{5}$$

$$\boldsymbol{u} = \boldsymbol{u_0} \quad \text{in } \Omega_0 \times t = t_0 \tag{6}$$

$$\dot{\boldsymbol{u}} = \dot{\boldsymbol{u}}_{\boldsymbol{0}} \quad \text{in } \Omega_0 \times t = t_0. \tag{7}$$

By adopting a Voigt notation which orders tensor components in an array according to the sequence of indices (11, 22, 33, 23, 31, 12), and under the assumption of cubic symmetry [46,47] which reduces Q_{ij} to Q_{11}, Q_{12} and Q_{44}, $\boldsymbol{E}^p$ can be expressed as:

$$E_1^p = Q_{11} p_1^2 + Q_{12}(p_2^2 + p_3^2) \tag{8}$$

$$E_2^p = Q_{11}p_2^2 + Q_{12}(p_1^2 + p_3^2)$$
$$E_3^p = Q_{11}p_3^2 + Q_{12}(p_1^2 + p_2^2)$$
$$E_4^p = Q_{44}p_2p_3$$
$$E_5^p = Q_{44}p_3p_1$$
$$E_6^p = Q_{44}p_1p_2.$$

Moreover, the electric field generated upon the application of a voltage difference V across the thin piezoelectric film thickness h oriented along direction 3, can be expressed as $\boldsymbol{E} = E\ \boldsymbol{e_3} = -(V/h)\ \boldsymbol{e_3}$ and a similar expression holds for the film polarization, *i.e.* $\boldsymbol{p} = p\ \boldsymbol{e_3}$. As a consequence, the inelastic strain components of Eq. (8), reduce to:

$$\begin{aligned} E_1^p &= E_2^p = Q_{12}p^2 \\ E_3^p &= Q_{11}p^2 \\ E_4^p &= E_5^p = E_6^p = 0. \end{aligned} \tag{9}$$

Under the hypothesis of transversal isotropy, the stress components of the piezoelectric thin film read:

$$\begin{aligned} S_1^p &= S_2^p = (A_{11}Q_{12} + A_{12}Q_{12} + A_{13}Q_{11})p^2 = \alpha_1 p^2 \\ S_3^p &= (A_{33}Q_{11} + 2A_{13}Q_{12})p^2 = \alpha_3 p^2. \end{aligned} \tag{10}$$

3.1.2. Weak formulation of motion

By exploiting the virtual work principle in the material form, the restricted weak formulation of the equations of motion can be obtained:

$$\int_{\Omega_0} \rho_0 \ddot{\boldsymbol{u}} \cdot \tilde{\boldsymbol{u}}\ d\Omega_0 + \int_{\Omega_0} \boldsymbol{P} : \nabla^T \tilde{\boldsymbol{u}}\ d\Omega_0 = 0 \qquad \forall \tilde{\boldsymbol{u}} \in C_u(0), \tag{11}$$

where $\tilde{\boldsymbol{u}}$ is a suitable test function belonging to the space $C_u(0)$ of functions that vanish on the boundary where Dirichlet boundary conditions are prescribed. By inserting the constitutive law in Eq. (11), it is obtained:

$$\int_{\Omega_0} \rho_0 \ddot{\boldsymbol{u}} \cdot \tilde{\boldsymbol{u}}\ d\Omega_0 + \int_{\Omega_0} \boldsymbol{E} : \mathcal{A} : \delta\boldsymbol{E}\ d\Omega_0 = \int_{\Omega_p} (\boldsymbol{S}^p - \boldsymbol{S_0}) : \delta\boldsymbol{E}\ d\Omega_0 \qquad \forall \tilde{\boldsymbol{u}} \in C_u(0), \tag{12}$$

where Ω_p is the piezoelectric domain and $\delta\boldsymbol{E} = sym(\nabla\tilde{\boldsymbol{u}}) + sym(\nabla^T\boldsymbol{u} \cdot \nabla\tilde{\boldsymbol{u}})$. The term $\int_{\Omega_0} \boldsymbol{E} : \mathcal{A} : \delta\boldsymbol{E}\ d\Omega_0$ describes geometric nonlinearities in terms of the unknown displacement field. By expanding Eq. (12), we obtain:

$$\begin{aligned} &\int_{\Omega_0} \rho_0 \ddot{\boldsymbol{u}} \cdot \tilde{\boldsymbol{u}}\ d\Omega_0 + \int_{\Omega_0} sym(\nabla\boldsymbol{u}) : \mathcal{A} : sym(\nabla\tilde{\boldsymbol{u}})\ d\Omega_0 + \\ &\int_{\Omega_0} sym(\nabla\boldsymbol{u}) : \mathcal{A} : sym(\nabla^T\tilde{\boldsymbol{u}} \cdot \nabla\boldsymbol{u})\ d\Omega_0 + \\ &\frac{1}{2}\int_{\Omega_0} sym(\nabla\tilde{\boldsymbol{u}}) : \mathcal{A} : sym(\nabla^T\boldsymbol{u} \cdot \nabla\boldsymbol{u})\ d\Omega_0 + \\ &\frac{1}{2}\int_{\Omega_0} sym(\nabla^T\boldsymbol{u} \cdot \nabla\boldsymbol{u}) : \mathcal{A} : sym(\nabla^T\tilde{\boldsymbol{u}} \cdot \nabla\boldsymbol{u})\ d\Omega_0 = \\ &\int_{\Omega_p} (\boldsymbol{S}^p - \boldsymbol{S}^0) : sym(\nabla\tilde{\boldsymbol{u}})\ d\Omega_p + \int_{\Omega_p} (\boldsymbol{S}^p - \boldsymbol{S}^0) : sym(\nabla^T\boldsymbol{u} \cdot \nabla\tilde{\boldsymbol{u}})\ d\Omega_p. \end{aligned} \tag{13}$$

Considering the left-hand-side, the first term represents the virtual work of inertia forces. The right-hand-side represents the virtual work of external forces due to the piezoelectric actuation. Upon addition of Rayleigh damping proportional to the mass matrix, the numerical solution of Eq. (13) can be obtained through a finite element space discretization with nodal shape functions [47] that leads to the time-dependent differential equations:

$$\boldsymbol{M}\ddot{\boldsymbol{U}} + \frac{\omega_0}{Q}\boldsymbol{M}\dot{\boldsymbol{U}} + \boldsymbol{F}(\boldsymbol{U}) = \boldsymbol{F_{in}}(t) + \boldsymbol{K_{in}}(t)\boldsymbol{U}, \tag{14}$$

where $\boldsymbol{M}$ represents the mass matrix, Q the quality factor, ω_0 the natural frequency, $\boldsymbol{F}(\boldsymbol{U})$ the nonlinear elastic force, $\boldsymbol{F_{in}}$ the forcing term and $\boldsymbol{K_{in}}$ the stiffness matrix induced by the time-dependent piezoelectric force and fabrication pre-stresses. It is worth noting that the chosen unipolar polarization histories generate polarization oscillations around a nonzero average value which has the same effect as a large pre-stress on the structure.

If T-periodic piezoelectric excitations are considered, it is possible to write:

$$\boldsymbol{F_{in}}(t) = \bar{\boldsymbol{F}}_{\boldsymbol{in}} + \tilde{\boldsymbol{F}}_{\boldsymbol{p}}(t) \tag{15a}$$

$$\boldsymbol{K_{in}}(t) = \bar{\boldsymbol{K}}_{\boldsymbol{in}} + \tilde{\boldsymbol{K}}_{\boldsymbol{p}}(t), \tag{15b}$$

where:

$$\bar{\boldsymbol{F}}_{\boldsymbol{in}} = \frac{1}{T}\int_0^T \boldsymbol{F_{in}}(t)\ dt, \tag{16a}$$

$$\bar{\boldsymbol{K}}_{\boldsymbol{in}} = \frac{1}{T}\int_0^T \boldsymbol{K}_{\boldsymbol{in}}(t)\, dt. \tag{16b}$$

Eq. (14) then becomes:

$$\boldsymbol{M}\ddot{\boldsymbol{U}} + \frac{\omega_0}{Q}\boldsymbol{M}\dot{\boldsymbol{U}} + (\boldsymbol{K} - \bar{\boldsymbol{K}}_{\boldsymbol{in}})\boldsymbol{U} + \boldsymbol{F}_{\boldsymbol{NL}}(\boldsymbol{U}) - \bar{\boldsymbol{F}}_{\boldsymbol{in}} = \tilde{\boldsymbol{F}}_p, \tag{17}$$

where the time dependent piezoelectric stiffness $\tilde{\boldsymbol{K}}_p(t)$ has been neglected according to what demonstrated in [47] and $\boldsymbol{F}(\boldsymbol{U}) = \boldsymbol{K}\boldsymbol{U} + \boldsymbol{F}_{\boldsymbol{NL}}(\boldsymbol{U})$ with $\boldsymbol{K}$ linear mechanical stiffness matrix.

The unknown displacement field $\boldsymbol{U}$ can then be decomposed in:

$$\boldsymbol{U}(t) = \boldsymbol{U}_{\boldsymbol{0}} + \tilde{\boldsymbol{U}}(t) \tag{18}$$

being $\boldsymbol{U}_{\boldsymbol{0}}$ the initial static configuration and $\tilde{\boldsymbol{U}}(t)$ its time dependent evolution. According to Eq. (17), the static problem that needs to be solved for $\boldsymbol{U}_{\boldsymbol{0}}$ reads:

$$(\boldsymbol{K} - \bar{\boldsymbol{K}}_{\boldsymbol{in}})\boldsymbol{U}_{\boldsymbol{0}} + \boldsymbol{F}_{\boldsymbol{NL}}(\boldsymbol{U}_{\boldsymbol{0}}) - \bar{\boldsymbol{F}}_{\boldsymbol{in}} = \boldsymbol{0}. \tag{19}$$

while the dynamic equations governing the nonlinear vibrations around the static position are:

$$\boldsymbol{M}\ddot{\tilde{\boldsymbol{U}}} + \frac{\omega_0}{Q}\boldsymbol{M}\dot{\tilde{\boldsymbol{U}}} + \boldsymbol{F}(\tilde{\boldsymbol{U}}) = \tilde{\boldsymbol{F}}_p. \tag{20}$$

3.1.3. Reduced order model

The full-order nonlinear model derived in the previous section is extremely computationally expensive and cannot be solved if design optimization must be performed. It is then here manipulated in order to make it exploitable for the LEM approach we want to employ in the following to estimate in a fast and effective way the MEMS loudspeaker THD.

The main idea is to derive a one-degree-of-freedom model able to reproduce the nonlinear electro-mechanical dynamic response of the MEMS loudspeaker. To do so, the pre-stressed undamped actuated mode of the structure, adimensionalized with unit maximum displacement, is chosen as test function $\boldsymbol{\Phi}$. Physical displacement, velocity and acceleration then read:

$$\tilde{\boldsymbol{u}}(\boldsymbol{x}) = \boldsymbol{\Phi}(\boldsymbol{x}) \tag{21}$$

$$\boldsymbol{u}(\boldsymbol{x}, t) = \boldsymbol{\Phi}(\boldsymbol{x})q(t) \tag{22}$$

$$\dot{\boldsymbol{u}}(\boldsymbol{x}, t) = \boldsymbol{\Phi}(\boldsymbol{x})\dot{q}(t) \tag{23}$$

$$\ddot{\boldsymbol{u}}(\boldsymbol{x}, \boldsymbol{t}) = \boldsymbol{\Phi}(\boldsymbol{x})\ddot{q}(t), \tag{24}$$

where $q(t)$ represents the modal coordinate that we will consider in the following as the system one degree of freedom. Note that, given the chosen adimensionalization of the eigenvector, it coincides with the maximum out-of-plane displacement of the MEMS loudspeaker diaphragm w.

According to this assumption, the inertia term of Eq. (20) can be rewritten as:

$$M_m\ddot{q}(t) = \int_\Omega \boldsymbol{\Phi}^T \rho \boldsymbol{\Phi}\, d\Omega\, \ddot{q}(t) \tag{25}$$

from which the modal mass M_m can be identified, while the damping term of the reduced order model reads $M_m\frac{\omega_0}{Q}\dot{q}$.

The piezoelectric force $\tilde{\boldsymbol{F}}_p$ can be also written in an explicit way considering the only non-zero components of inelastic stresses (see Eq. (10)) as:

$$r_P p^2(V(t)) = \int_{\Omega_p} [\alpha_1(\varepsilon_1[\boldsymbol{\Phi}] + \varepsilon_2[\boldsymbol{\Phi}]) + \alpha_3\varepsilon_3[\boldsymbol{\Phi}]]\, d\Omega_p\, p^2(V(t)), \tag{26}$$

where $\varepsilon_i = \dfrac{\partial u_i}{\partial x_i}$ represent the standard components of the small strain tensor and r_P the participating piezoelectric coefficient.

To numerically compute the loudspeaker pre-stressed mechanical mode, a modal analysis that considers as reference configuration the pre-deflected shape of the speaker induced by fabrication process pre-stresses and by the applied Direct Current (DC) voltage, is performed in COMSOL Multiphysics® v6.1, as illustrated in Fig. 3. In practical terms, the quantities extracted from the numerical eigenfrequency study in COMSOL Multiphysics® are the first eigenvector $\boldsymbol{\Phi}$, the corresponding eigenvalue ω_0^2, the strain components $\varepsilon_1(\boldsymbol{\Phi})$, $\varepsilon_2(\boldsymbol{\Phi})$ and $\varepsilon_3(\boldsymbol{\Phi})$, and the integral quantities M_m and r_P.

The implicit static condensation technique [63,64], recently tailored for MEMS applications [65,66], is finally applied to reduce the dimensions of the nonlinear elastic term $\boldsymbol{F}(\boldsymbol{U})$. The above mentioned technique relies on the evaluation of the nonlinear elastic force by statically forcing the structure with body forces F proportional to $\boldsymbol{\Phi}$: $F = \rho_0\beta\boldsymbol{\Phi}(\boldsymbol{x})$.

A series of numerical static non-linear analyses are run spanning the β space and computing the corresponding modal coordinate, thus identifying the $q(\beta)$ relation that can be easily numerically inverted through fitting procedures (Fig. 3):

$$\beta(q) = k_1 q + k_2 q^2 + k_3 q^3. \tag{27}$$

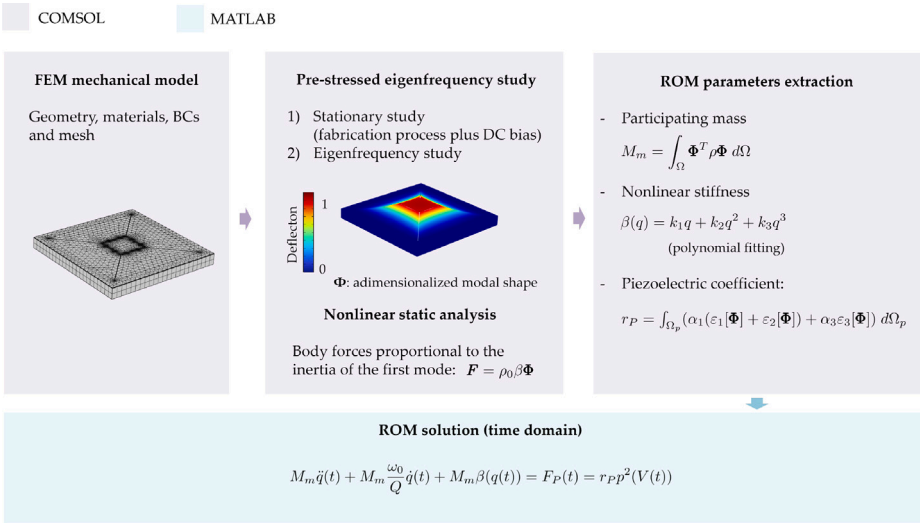

Fig. 3. Flowchart of the ROM parameters extraction from a pre-stressed modal analysis and a nonlinear static analysis computed via FEM in COMSOL Multiphysics® v6.1. The ROM model is then solved in terms of loudspeaker displacement and velocity in MATLAB R2022a, through the MATCONT package [67].

The corresponding one-degree-of-freedom equation describing the nonlinear vibrations of the loudspeaker around the static configuration $\boldsymbol{U_0}$ can be written as:

$$\ddot{q}(t) + \frac{\omega_0}{Q}\dot{q}(t) + \beta(q(t)) = \frac{r_P p^2(t)}{M_m} \tag{28}$$

and solved in terms of loudspeaker displacement and velocity through periodic orbits numerical continuation tools, like e.g. the MATCONT package [67].

3.2. Coupling with acoustics

The acoustic domain can be modelled through a linear equivalent circuit. In this work, the circuit reported in Fig. 2(b) for the case of radiation in an IEC 60318-4 ear simulator is considered. The interested reader can refer to [9] for the parameters values and its full derivation.

We here focus on the coupling between such linear model, which works in the frequency domain, with the nonlinear electro-mechanical one derived in the previous section.

Firstly, the nonlinear time-dependent velocity $\dot{q} = v$ is decomposed in Fourier series retaining n harmonic components:

$$\dot{q}(t) = v(t) = \sum_{i=1}^{n} v_i(f) e^{ji\omega t}, \tag{29a}$$

$$v_i(f) = \frac{2}{T}\int_0^T v(t) e^{-ji\omega t}. \tag{29b}$$

Secondly, each velocity harmonic component v_i, upon multiplication by the speaker effective area, is imposed as current source to each of the n equivalent circuits working at circular frequencies $\omega_i = i\omega$, $i = 1, \dots, n$.

The equivalent acoustic impedance Z_a can be derived from the reported equivalent network:

$$Z_a = \frac{1}{\frac{1}{R_s} + \frac{1}{\frac{1}{j\omega_i C_{bc}} + Z_{es}}}, \tag{30}$$

where Z_{es} represents the ear simulator input impedance, which can be expressed as:

$$Z_{es} = j\omega_i L_1 + \frac{1}{\frac{1}{Z_1} + \frac{1}{Z_2} + \frac{1}{j\omega_i L_3 + \frac{1}{\frac{1}{Z_3} + \frac{1}{Z_4} + \frac{1}{Z_5}}}}, \tag{31}$$

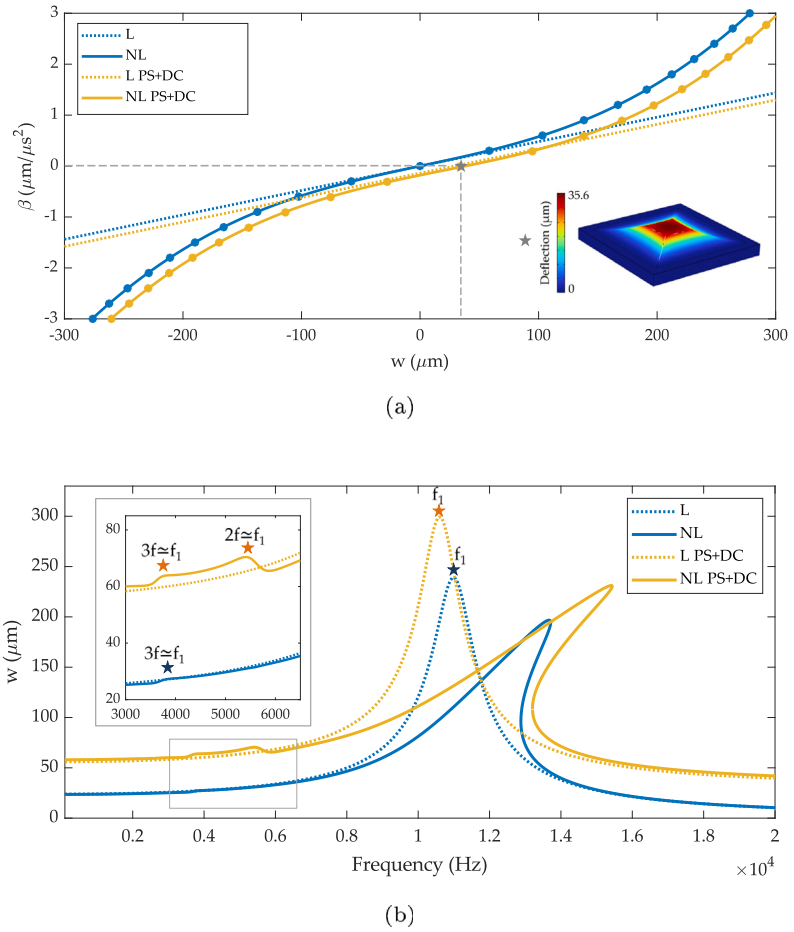

Fig. 4. (a) Nonlinear load multiplier β versus maximum out-of-plane displacement w numerically computed for the case without pre-stresses induced by the fabrication process and DC voltage (light blue line) and including them (orange line). The reference linear cases (dotted lines) are also reported for the sake of clarity. The static initial deformed shape ($\beta = 0$) is reported in the inset. (b) Frequency response function in terms of diaphragm displacement numerically computed under a linear piezoelectric forcing term and for a Q = 10 (see Appendix) when pre-stresses are considered (yellow solid line) and neglected (light blue solid line).

with $Z_1 = R_1 + \frac{1}{j\omega_i C_1}$, $Z_2 = j\omega_i L_2 + \frac{1}{j\omega_i C_2} + R_2$, $Z_3 = R_3 + \frac{1}{j\omega_i C_3}$, $Z_4 = j\omega_i L_4 + \frac{1}{j\omega_i C_4} + R_4$ and $Z_5 = j\omega_i L_5 + \frac{1}{j\omega_i C_5}$. The transfer function $T_a = p_{out,i}/p_{in,i}$ can be written as:

$$T_a = \frac{Z_{es}}{\frac{1}{j\omega_i C_{bc}} + Z_{es}} T_{es}, \tag{32}$$

where T_{es} is the ear simulator transfer function which reads:

$$T_{es} = \frac{Z_{es} - j\omega_i L_1}{Z_{es}} \frac{\frac{1}{\frac{1}{Z_3} + \frac{1}{Z_4} + \frac{1}{Z_5}}}{j\omega_i L_3 + \frac{1}{\frac{1}{Z_3} + \frac{1}{Z_4} + \frac{1}{Z_5}}} \frac{1}{j\omega_i C_5 Z_5}. \tag{33}$$

The output pressures $p_{out,i}$ is then retrieved from the velocity v_i and the transfer function T_a as:

$$p_{out,i} = T_a p_{in,i} = T_a Q_i Z_a = T_a S_{eff} v_i Z_a, \tag{34}$$

and the THD is finally computed through:

$$THD_{\%} = \frac{\sqrt{\sum_{i=2}^{n} p_{out,i}^2}}{p_{out,1}} \cdot 100. \tag{35}$$

4. Numerical results

The proposed nonlinear reduced model is here employed to compute the response of the reference MEMS loudspeaker presented in Section 2.

Firstly, the load multiplier β is computed according to the implicit static condensation method explained in Section 3.1.3 for different values of the diaphragm out-of-plane maximum displacement w by running a set of nonlinear static analyses in COMSOL Multiphysics® v6.1. In Fig. 4(a), the numerically computed $\beta(w)$ curve is reported for both the linear (L in Fig. 4(a)) and nonlinear (NL in Fig. 4(a)) cases in presence and in absence of fabrication induced pre-stresses (PS in Fig. 4(a)) and Direct Current (DC) voltage pre-deflection (DC in Fig. 4(a)). FEM results are reported in dots, while cubic interpolation curves are reported in continuous lines. The identified mechanical stiffness nonlinear coefficients (Eq. (27)) are reported in Appendix. As expected, in presence of a diaphragm pre-deflection, the $\beta = 0$ condition corresponds to a non-zero displacement of the MEMS loudspeaker (see inset of Fig. 4(a)).

To better underline the effect of geometric nonlinearities on the MEMS loudspeaker dynamic response, we report in Fig. 4(b), the frequency response function computed by integrating Eq. (28) under the four above mentioned conditions, *i.e.* L, L DC+PS, NL and NL DC+PS and for Q = 10 (see Appendix). The latter has been tuned in [19] to match the experimental SPL peak amplitude at the speaker resonance frequency.

Note that the piezoelectric forcing term is here considered according to the piezoelectric linear formulation [19] in order to decouple the nonlinear sources and then simplify the physical interpretation of the results. From Fig. 4(b) it is clear that geometric nonlinearities are hardening in nature and that pre-stresses and DC pre-deflections cause a shift of the natural frequency towards higher values. Moreover, it is worth noting that a $3f \cong f_1$ peak appears as a consequence of the cubic geometric nonlinear term and a $2f \cong f_1$ peak arises because of the symmetry breakdown caused by the deformed initial configuration, *i.e.* quadratic nonlinearities.

The P2-formulation, described in Section 3.1.1, is then considered in the definition of the piezoelectric forcing term in order to provide a complete electro-mechanical MEMS loudspeaker frequency response prediction. In particular, to derive the piezoelectric terms of Eq. (28), the experimental unipolar hysteresis loop (Fig. 5(a) left) measured at 30 V on the reference speaker fabricated by STMicroelectronics is experimentally measured with the set-up described in [68]. The corresponding periodic polarization history, decomposed in Fourier series retaining five harmonics, is also derived and reported on the right side of Fig. 5(a) for the sake of clarity. In Fig. 5(b), the frequency response function numerically computed in terms of diaphragm displacement for Q = 10 (see Appendix) through Eq. (28), is reported under three different conditions: *(i)* linear piezoelectric formulation and no geometric nonlinearities (dotted orange line), *(ii)* P2-formulation and no geometric nonlinearities (dotted violet line) and *(iii)* P2-formulation and geometric nonlinearities (solid violet line). As expected from the nonlinear content of the polarization curves reported in Fig. 5(a), subharmonics peaks appear at $5f \cong f_1$, $4f \cong f_1$, $3f \cong f_1$ and $2f \cong f_1$.

To complete the numerical prediction of the MEMS loudspeaker nonlinear response, we here introduce the coupling with the acoustic domain. Note that, the above mentioned harmonics coming from the electro-mechanical nonlinear model, *i.e.* polarization curve that introduces a five-harmonics forcing term and geometric nonlinearities which introduce quadratic and cubic terms in the mechanical stiffness of the one-degree-of-freedom model, are fully transferred to the linear acoustic domain. Peaks at $f_1/2$, $f_1/3$, $f_1/4$ and $f_1/5$ are then expected in the MEMS loudspeaker acoustic response.

In Fig. 6 the frequency response function computed in terms of diaphragm out-of-plane displacement is reported for the device under study coupled with the coupler and a 1 cm^3 back chamber. To support the hypothesis done in Section 3.2, *i.e.* negligible acoustic load effect on the speaker dynamic response, we report in Fig. 6 the two curves computed by considering and neglecting such contribution. The acoustic load adds an additional damping at resonance and a small shift in terms of loudspeaker resonance frequency. However, for the device under study, such discrepancies can be considered negligible and the chosen hypothesis fully satisfied as also demonstrated in Fig. 6(b) where the SPL curve is reported by considering and not considering the acoustic load.

The computed THD is finally reported in Fig. 7 under different hypotheses: *(i)* geometric nonlinearities and linear piezoelectric formulation, *(ii)* P2-formulation for piezoelectricity and no geometric nonlinearities and *(iii)* P2-formulation for piezoelectricity and geometric nonlinearities. From Fig. 7, it is clear that the piezoelectric hysteretical behaviour is the major source of THD.

5. Experimental results

To validate the proposed nonlinear reduced order model, acoustic tests are performed for in-ear conditions on the reference MEMS loudspeaker fabricated by STMicroelectronics.

In particular, as shown in Fig. 8(a), the device is mounted on a custom Printed Circuit Board (PCB) and coupled with an ABS (Acrylonitrile Butadiene Styrene) thermoplastic package made by a 1 cm^3 back chamber and a 1 mm high front adapter properly shaped to connect the speaker with the ear simulator. The employed experimental set-up, schematized in Fig. 8(b), includes the anechoic chamber G.R.A.S. AL0030-S2, the ear simulator G.R.A.S. RA0402 and the microphone G.R.A.S. 46 BD $\frac{1}{4}''$. DC and AC

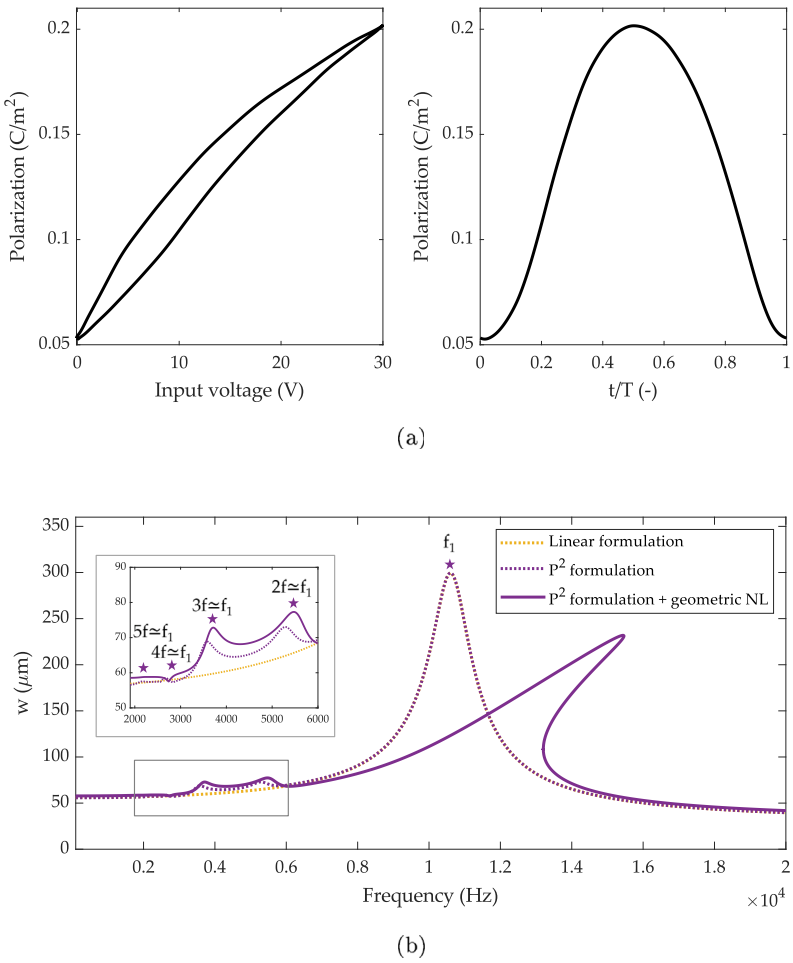

Fig. 5. (a) Unipolar experimental hysteresis loop at 30 V (left) and corresponding periodic polarization history, decomposed in Fourier series retaining five harmonics (right) (b) Displacement FRF considering the nonlinear piezoelectric forcing term only (dotted violet line) and the nonlinear piezoelectric forcing term plus geometric nonlinearities (solid violet line). The reference FRF considering the standard linear piezoelectricity is reported with dotted orange line for the sake of clarity.

signals needed for the diaphragm actuation and conversion of the microphone signal into SPL data, are finally generated through the Audio Analyzer (APx525).

Experimental SPL and THD curves measured on six nominally identical prototypes are reported in Fig. 9 for an AC voltage of 30 V_{pp} and a bias voltage of 12.5 V_{DC}. The mean experimental value is reported with a red solid line, while the standard deviation is indicated by the pink shaded area. The acquisition is stopped at 10 kHz to avoid the break-up of the prototypes.

Note that, as anticipated in Section 3.1.1, to limit piezoelectric domains re-orientation and hence hysteresis, AC voltage amplitude should be equal to twice the DC voltage during the device actuation, thus avoiding electric field sign changes. Here, the AC and DC voltages amplitudes do not exactly satisfy such requirement due to experimental set-up limitations. However, despite the proposed working condition is not optimal for the maximization of the loudspeaker performances in terms of THD, it does not compromise the main goal of this work which is to prove the predictability of the proposed nonlinear reduced order model.

The experimental SPL results of Fig. 9(a) have been already analysed and compared with the linear model in [19]. The good agreement between the two curve is here confirmed, as expected. In Fig. 9(b), experimental THD curves are instead compared with numerical predictions obtained through the proposed nonlinear reduced order model for the first time. The subharmonics peaks position are correctly captured along with the level in the quasi-static region, thus demonstrating a very good predictability of the proposed model. The discrepancy in the THD level at subharmonics frequencies can be partially justified by the employed

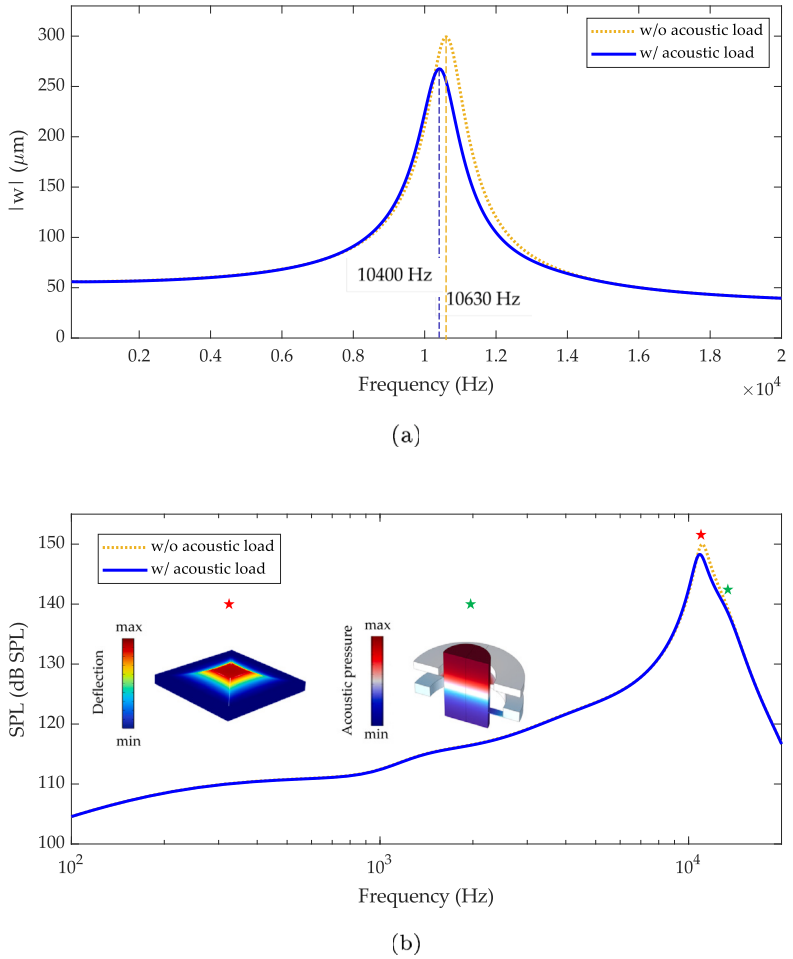

Fig. 6. (a) Linear FRF by considering the acoustic load (solid blue line) due to the ear simulator and a back chamber of 1 cm^3 and by neglecting it (dotted orange line). The corresponding SPL is reported in subfigure (b).

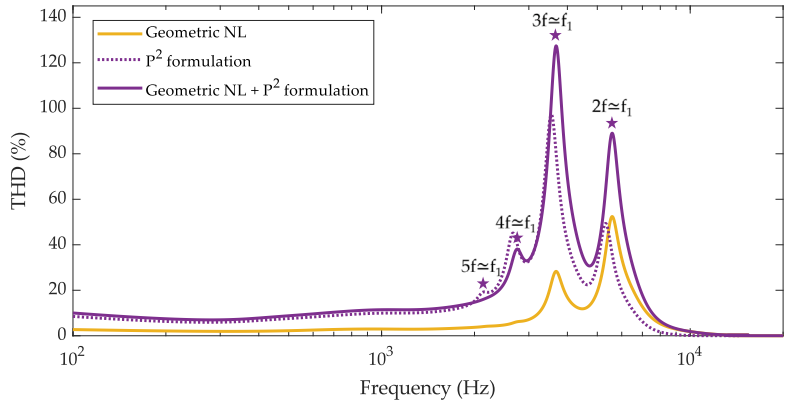

Fig. 7. THD contributions of geometric nonlinearities (solid orange line), nonlinear piezoelectric force (dashed violet line) and considering both the nonlinear effects (solid violet line).

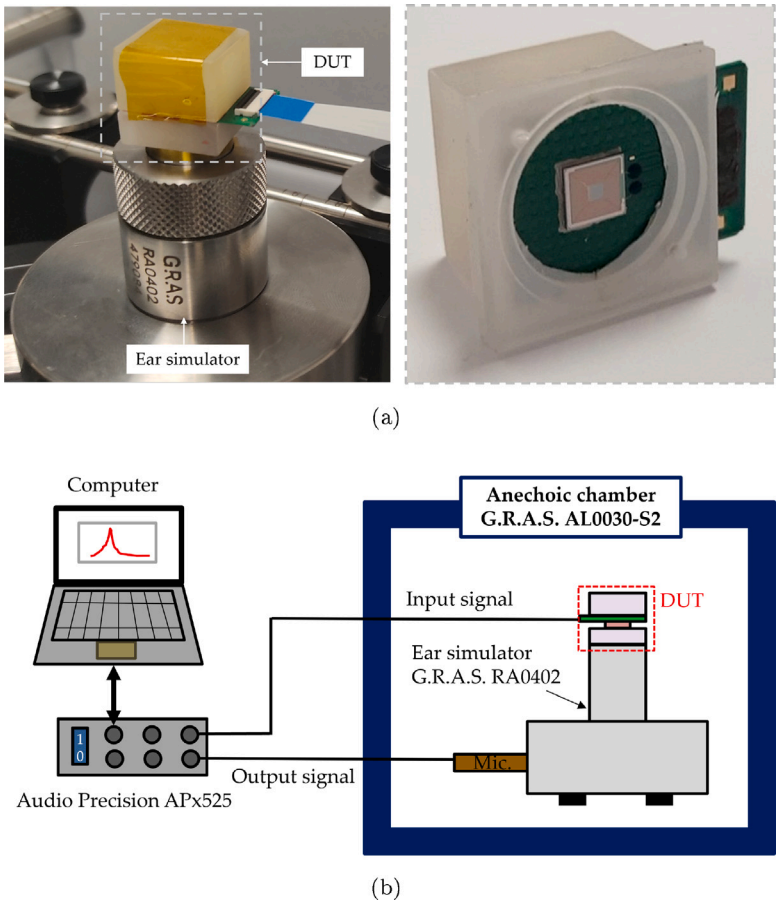

Fig. 8. (a) Device under test coupled with the ear simulator. A close-up view of the fabricated loudspeaker mounted on a custom PCB and coupled with the package for in-ear acoustic tests is also reported. (b) Acoustic measurement set-up composed of the ear simulator G.R.A.S. RA0402 and the microphone G.R.A.S. 46 BD 1/4″. The Audio Analyzer (APx525) allows to generate DC and AC signals for the MEMS actuation and to convert the microphone signal into SPL data.

hypothesis on the one-way electro-mechanics vs. acoustics coupling, which results in neglecting the damping contribution coming from the acoustic load (see Fig. 6).

6. Conclusions

A nonlinear model able to predict the THD of a piezoelectric MEMS loudspeaker has been presented and experimentally validated. To the Authors best knowledge, it is the first model proposed in the literature including both the effect of geometric nonlinearities and piezoelectric hysteresis able to reproduce the THD response of a MEMS piezoelectric loudspeaker.

Despite being presented and validated for in-ear conditions, it can be straightforwardly applied for the THD prediction for free-field conditions, by simply replacing the acoustic equivalent circuit with the one representing the radiation in an unbounded domain [69]. Moreover, the versatility of the proposed approach lies in the FEM assisted extraction of the electro-mechanical parameters that allows to accurately model loudspeaker diaphragms of arbitrarily complex geometry.

Future work will be addressed to the implementation of the two-way coupling between the electro-mechanical and the acoustic domains. The acoustic load coming for example from small back chambers can indeed have a definitively not negligible influence on the loudspeaker frequency response. Moreover, a more detailed estimation of the system damping is needed in order to make the proposed nonlinear model universal for every MEMS loudspeaker.

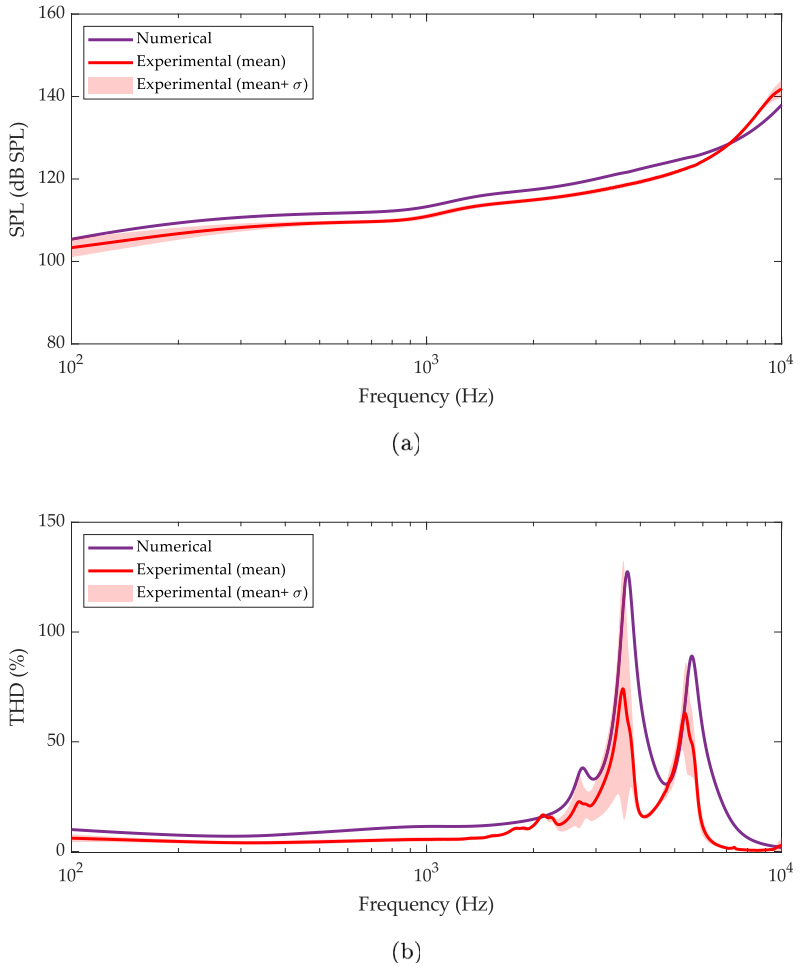

Fig. 9. Comparison between numerical (violet curves) and experimental (mean value in red and standard deviation in pink shaded areas) (a) SPL and (b) THD frequency spectra at 30 V_{pp}. The acquisition is stopped at 10 kHz to avoid the break-up of the prototypes.

CRediT authorship contribution statement

Chiara Gazzola: Writing – review & editing, Writing – original draft, Software, Methodology, Formal analysis, Data curation, Conceptualization. **Alberto Corigliano:** Writing – review & editing, Funding acquisition. **Valentina Zega:** Writing – review & editing, Writing – original draft, Project administration, Conceptualization.

Declaration of competing interest

The authors declare the following financial interests/personal relationships which may be considered as potential competing interests: Alberto Corigliano reports financial support was provided by JRP-STEAM STMicroelectronics-Politecnico di Milano. Valentina Zega reports financial support was provided by JRP-STEAM STMicroelectronics-Politecnico di Milano. Chiara Gazzola reports financial support was provided by JRP-STEAM STMicroelectronics-Politecnico di Milano. If there are other authors, they declare that they have no known competing financial interests or personal relationships that could have appeared to influence the work reported in this paper.

Data availability

Data will be made available on request.

Acknowledgements

The authors would like to thank STMicroelectronics for the fabrication of the prototypes and in particular Dr. Fabrizio Cerini for the precious contribution in the experimental campaign. C.G. and V.Z. are grateful to Dr. Giorgio Gobat for insightful discussions on geometric nonlinearities and reduced order models. The research has been funded by the JRP-STEAM STMicroelectronics-Politecnico di Milano.

Appendix

Parameters employed in the Reduced Order Model presented in this work are reported in Table 1.

Table 1
Parameters of electro-mechanical ROM.

Parameter	Value	Unit
M_m	$9.94 \cdot 10^{-8}$	kg
Q	10	–
k_1	$5.55 \cdot 10^{9}$	s^{-2}
k_2	$-3.04 \cdot 10^{13}$	$m^{-1}\ s^{-2}$
k_3	$3.24 \cdot 10^{17}$	$m^{-2}\ s^{-2}$
r_p	0.612	$N\ m^4\ C^{-2}$

References

[1] A. Rusconi, S. Costantini, C. Prelini, Micro speakers, in: Silicon Sensors and Actuators, Springer, 2022, pp. 651–676.
[2] D. Beer, A. Mannchen, T. Fritsch, J. Kuller, A. Zhykhar, G. Fischer, F.M. Fiedler, Expedition MEMS speaker, in: Forum Acusticum, 2020, pp. 2921–2928.
[3] H. Wang, Y. Ma, Q. Zheng, K. Cao, Y. Lu, H. Xie, Review of recent development of MEMS speakers, Micromachines 12 (10) (2021) 1257.
[4] M.V. Garud, R. Pratap, MEMS audio speakers, J. Micromech. Microeng. (2023).
[5] R. Liechti, S. Durand, T. Hilt, F. Casset, C. Dieppedale, M. Colin, High performance piezoelectric MEMS loudspeaker based on an innovative wafer bonding process, Sensors Actuators A 358 (2023) 114413.
[6] H. Wang, Z. Chen, H. Xie, A high-SPL piezoelectric MEMS loud speaker based on thin ceramic PZT, Sensors Actuators A 309 (2020) 112018.
[7] M.V. Garud, R. Pratap, A novel MEMS speaker with peripheral electrostatic actuation, J. Microelectromech. Syst. 29 (4) (2020) 592–599.
[8] I. Shahosseini, E. Lefeuvre, J. Moulin, E. Martincic, M. Woytasik, G. Lemarquand, Optimization and microfabrication of high performance silicon-based MEMS microspeaker, IEEE Sens. J. 13 (1) (2012) 273–284.
[9] C. Gazzola, V. Zega, F. Cerini, S. Adorno, A. Corigliano, On the design and modeling of a full-range piezoelectric MEMS loudspeaker for in-ear applications, J. Microelectromech. Syst. (2023) 1–12, (published online).
[10] B. Kaiser, H.A.G. Schenk, L. Ehrig, F. Wall, J.M. Monsalve, S. Langa, M. Stolz, A. Melnikov, H. Conrad, D. Schuffenhauer, H. Schenk, The push-pull principle: an electrostatic actuator concept for low distortion acoustic transducers, Microsyst. Nanoeng. 8 (1) (2022) 1–14.
[11] F. Stoppel, A. Männchen, F. Niekiel, D. Beer, T. Giese, B. Wagner, New integrated full-range MEMS speaker for in-ear applications, in: 2018 IEEE Micro Electro Mechanical Systems, MEMS, 2018, pp. 1068–1071, ISSN: 2160-1968.
[12] T.-C. Wei, Z.-S. Hu, S.-W. Chang, W. Fang, On the design of piezoelectric MEMS microspeaker with high fidelity and wide bandwidth, in: 2023 IEEE 36th International Conference on Micro Electro Mechanical Systems, MEMS, IEEE, 2023, pp. 127–130.
[13] Y.-C. Chen, H.-H. Cheng, M.-C. Cheng, S.-C. Lo, C.-K. Chan, W. Fang, On the design of a two-way piezoelectric MEMS microspeaker based on a multi-shape cantilever array for high-frequency applications, J. Micromech. Microeng. 33 (7) (2023) 074001.
[14] C. Gazzola, V. Zega, F. Cerini, S. Adorno, A. Corigliano, On the design and modeling of a full-range piezoelectric MEMS loudspeaker for in-ear applications, J. Microelectromech. Syst. (2023).
[15] H.-H. Cheng, S.-C. Lo, Z.-R. Huang, Y.-J. Wang, M. Wu, W. Fang, On the design of piezoelectric MEMS microspeaker for the sound pressure level enhancement, Sensors Actuators A 306 (2020) 111960.
[16] C. Gazzola, V. Zega, A. Corigliano, L. Pierrick, M. Melon, Lumped-parameters equivalent circuit for piezoelectric MEMS speakers modeling, in: Forum Acusticum, 2023.
[17] S. Zhao, X. Qiu, I. Burnett, M. Rigby, A. Lele, A lumped-parameter model for sound generation in gas metal arc welding, Mech. Syst. Signal Process. 147 (2021) 107085.
[18] R. Liechti, S. Durand, T. Hilt, F. Casset, M. Colin, MEMS loudspeaker for in-ear application, 2023.
[19] C. Gazzola, V. Zega, A. Corigliano, L. Pierrick, M. Melon, A reduced-order-model-based equivalent circuit for piezoelectric MEMS loudspeakers modeling, J. Acoust. Soc. Amer. 155 (2) (2024) 1503–1514, http://dx.doi.org/10.1121/10.0024939.
[20] S.-H. Tseng, S.-C. Lo, Y.-J. Wang, S.-W. Lin, M. Wu, W. Fang, Sound pressure and low frequency enhancement using novel PZT MEMS microspeaker design, in: 2020 IEEE 33rd International Conference on Micro Electro Mechanical Systems, MEMS, 2020, pp. 546–549.
[21] Y. Ma, Y. Lu, N. Deng, Q. Zheng, K. Cao, H. Wang, H. Xie, A PZT MEMS loudspeaker with a quasi-closed diaphragm, Sensors Actuators A 358 (2023) 114454.
[22] L. Xu, M. Sun, M. Zhang, C. Liu, X. Yang, W. Pang, A piezoelectric MEMS speaker with stretchable film sealing, in: 2023 IEEE 36th International Conference on Micro Electro Mechanical Systems, MEMS, IEEE, 2023, pp. 673–676.
[23] S. van Ophem, W. Desmet, Physics-based sound radiation estimation from multiple speakers by combined lumped parameter and reduced-order finite element modeling, Mech. Syst. Signal Process. 167 (2022) 108585.
[24] W. Klippel, Tutorial: Loudspeaker nonlinearities—Causes, parameters, symptoms, J. Audio Eng. Soc. 54 (10) (2006) 907–939.
[25] M. Rébillat, R. Hennequin, E. Corteel, B.F. Katz, Identification of cascade of Hammerstein models for the description of nonlinearities in vibrating devices, J. Sound Vib. 330 (5) (2011) 1018–1038.
[26] A. King, F. Agerkvist, Fractional derivative loudspeaker models for nonlinear suspensions and voice coils, J. Audio Eng. Soc. 66 (7/8) (2018) 525–536.
[27] J.M. Monsalve, A. Melnikov, B. Kaiser, D. Schuffenhauer, M. Stolz, L. Ehrig, H.A. Schenk, H. Conrad, H. Schenk, Large-signal equivalent-circuit model of asymmetric electrostatic transducers, IEEE/ASME Trans. Mechatronics 27 (5) (2021) 2612–2622.
[28] A. Novak, L. Simon, P. Lotton, B. Merit, J. Gilbert, Nonlinear analysis and modeling of electrodynamic loudspeakers, in: 10ème Congrès Français d'Acoustique, 2010.

[29] A. Falaize, N. Papazoglou, T. Hélie, N. Lopes, Compensation of loudspeaker's nonlinearities based on flatness and port-Hamiltonian approach, in: 22ème Congrès Français de Mécanique, 2015.
[30] R. Ravaud, G. Lemarquand, T. Roussel, Time-varying non linear modeling of electrodynamic loudspeakers, Appl. Acoust. 70 (3) (2009) 450–458.
[31] A. Falaize, T. Hélie, Passive modelling of the electrodynamic loudspeaker: from the Thiele–Small model to nonlinear port-Hamiltonian systems, Acta Acust. 4 (1) (2020) 1.
[32] S. Temme, P. Brunet, A new method for measuring distortion using a multitone stimulus and noncoherence, J. Audio Eng. Soc. 56 (3) (2008) 176–188.
[33] P. Brunet, B. Shafai, New trends in modeling and identification of loudspeaker with nonlinear distortion, in: Proceedings of the International Conference on Modeling, Simulation and Visualization Methods, MSV, The Steering Committee of The World Congress in Computer Science, Computer . . . , 2011, p. 1.
[34] A.J. Kaizer, Modeling of the nonlinear response of an electrodynamic loudspeaker by a Volterra series expansion, J. Audio Eng. Soc. 35 (6) (1987) 421–433.
[35] K. Lashkari, A novel volterra-wiener model for equalization of loudspeaker distortions, in: 2006 IEEE International Conference on Acoustics Speech and Signal Processing Proceedings, Vol. 5, IEEE, 2006, p. V.
[36] W. Klippel, Modeling the large signal behavior of micro-speakers, in: Audio Engineering Society Convention 133, Audio Engineering Society, 2012.
[37] G.-Y. Hwang, H.-G. Kim, S.-M. Hwang, B.-S. Kang, Analysis of harmonic distortion due to uneven magnetic field in a microspeaker used for mobile phones, IEEE Trans. Magn. 38 (5) (2002) 2376–2378.
[38] S. Weng, S. Pawar, J.H. Huang, Magnetic motor nonlinearity modifications for total harmonic distortion improvement of an elliptical miniature loudspeaker, IEEE Trans. Magn. 48 (12) (2012) 4811–4814.
[39] C. Chang, S. Pawar, S. Weng, Y. Shiah, J.H. Huang, Effect of nonlinear stiffness on the total harmonic distortion and sound pressure level of a circular miniature loudspeaker-experiments and simulations, IEEE Trans. Consum. Electron. 58 (2) (2012) 212–220.
[40] S. Pawar, S. Weng, J.H. Huang, Total harmonic distortion improvement for elliptical miniature loudspeaker based on suspension stiffness nonlinearity, IEEE Trans. Consum. Electron. 58 (2) (2012) 221–227.
[41] C. Sun, F. An, B. Liu, S. Wu, The prediction of nonlinear resistance and distortion for a miniature loudspeaker with vented cavities, J. Acoust. Soc. Am. 146 (6) (2019) 4315–4321.
[42] J. Huang, X. Feng, S. Chen, Y. Shen, Analysis of total harmonic distortion of miniature loudspeakers used in mobile phones considering nonlinear acoustic damping, J. Acoust. Soc. Am. 149 (3) (2021) 1579–1588.
[43] B. Kaiser, S. Langa, L. Ehrig, M. Stolz, H. Schenk, H. Conrad, H. Schenk, K. Schimmanz, K. Schimmanz, D. Schuffenhauer, Concept and proof for an all-silicon MEMS micro speaker utilizing air chambers, Microsyst. Nanoeng. 5 (43) (2019).
[44] R. Liechti, S. Durand, T. Hilt, F. Casset, C. Poulain, G. Le Rhun, F. Pavageau, H. Kuentz, M. Colin, Total harmonic distortion of a piezoelectric MEMS loudspeaker in an IEC 60318-4 coupler estimation using static measurements and a nonlinear state space model, Micromachines 12 (12) (2021) 1437.
[45] R. Liechti, Development of a MEMS Loudspeaker with Optimized Performance (These de doctorat), Le Mans, 2022, URL https://www.theses.fr/2022LEMA1037.
[46] A. Frangi, A. Opreni, N. Boni, P. Fedeli, R. Carminati, M. Merli, G. Mendicino, Nonlinear response of PZT-actuated resonant micromirrors, J. Microelectromech. Syst. 29 (6) (2020) 1421–1430.
[47] A. Opreni, G. Gobat, C. Touzé, A. Frangi, Nonlinear model order reduction of resonant piezoelectric micro-actuators: An invariant manifold approach, Comput. Struct. 289 (2023) 107154.
[48] A. Opreni, N. Boni, R. Carminati, A. Frangi, Analysis of the nonlinear response of piezo-micromirrors with the harmonic balance method, Actuators 10 (2) (2021).
[49] A. Opreni, N. Boni, G. Mendicino, M. Merli, R. Carminati, A. Frangi, Modeling material nonlinearities in piezoelectric films: quasi-static actuation, in: 2021 IEEE 34th International Conference on Micro Electro Mechanical Systems, MEMS, IEEE, 2021, pp. 85–88.
[50] M. Kamlah, C. Tsakmakis, Phenomenological modeling of the non-linear electro-mechanical coupling in ferroelectrics, Int. J. Solids Struct. 36 (5) (1999) 669–695.
[51] V. Mehling, C. Tsakmakis, D. Gross, Phenomenological model for the macroscopical material behavior of ferroelectric ceramics, J. Mech. Phys. Solids 55 (10) (2007) 2106–2141.
[52] J. Huber, Micromechanical modelling of ferroelectrics, Curr. Opin. Solid State Mater. Sci. 9 (3) (2005) 100–106.
[53] J. Wang, S.-Q. Shi, L.-Q. Chen, Y. Li, T.-Y. Zhang, Phase-field simulations of ferroelectric/ferroelastic polarization switching, Acta Mater. 52 (3) (2004) 749–764.
[54] Y. Su, C.M. Landis, Continuum thermodynamics of ferroelectric domain evolution: Theory, finite element implementation, and application to domain wall pinning, J. Mech. Phys. Solids 55 (2) (2007) 280–305.
[55] D. Schrade, R. Müller, B.-X. Xu, D. Gross, Domain evolution in ferroelectric materials: A continuum phase field model and finite element implementation, Comput. Methods Appl. Mech. Engrg. 196 (41–44) (2007) 4365–4374.
[56] X. Zhang, Y. Tan, M. Su, Modeling of hysteresis in piezoelectric actuators using neural networks, Mech. Syst. Signal Process. 23 (8) (2009) 2699–2711.
[57] F. Qian, L.S. da Silva, Y. Liao, L. Zuo, Statistical linearization for random vibration energy harvesting with piezoelectric material nonlinearity, Mech. Syst. Signal Process. 188 (2023) 109985.
[58] A review on control strategies for compensation of hysteresis and creep on piezoelectric actuators based micro systems, Mech. Syst. Signal Process. 140 (2020) 106634.
[59] A. Devonshire, Theory of ferroelectrics, Adv. Phys. 3 (10) (1954) 85–130.
[60] S. Trolier-McKinstry, P. Muralt, Thin film piezoelectrics for MEMS, J. Electroceram. 12 (2004) 7–17.
[61] M.J. Haun, E. Furman, S. Jang, H. McKinstry, L. Cross, Thermodynamic theory of PbTiO3, J. Appl. Phys. 62 (8) (1987) 3331–3338.
[62] P. Fedeli, M. Kamlah, A. Frangi, Phase-field modeling of domain evolution in ferroelectric materials in the presence of defects, Smart Mater. Struct. 28 (3) (2019) 035021.
[63] M. McEwan, J. Wright, J. Cooper, A. Leung, A finite element/modal technique for nonlinear plate and stiffened panel response prediction, in: 19th AIAA Applied Aerodynamics Conference.
[64] J.J. Hollkamp, R.W. Gordon, Reduced-order models for nonlinear response prediction: Implicit condensation and expansion, J. Sound Vib. 318 (4) (2008) 1139–1153.
[65] V. Zega, G. Gattere, S. Koppaka, A. Alter, G.D. Vukasin, A. Frangi, T.W. Kenny, Numerical modelling of non-linearities in MEMS resonators, J. Microelectromech. Syst. 29 (6) (2020) 1443–1454.
[66] A. Frangi, G. Gobat, Reduced order modelling of the non-linear stiffness in MEMS resonators, Int. J. Non-Linear Mech. 116 (2019) 211–218.
[67] A. Dhooge, W. Govaerts, Y.A. Kuznetsov, MATCONT: a MATLAB package for numerical bifurcation analysis of ODEs, ACM Trans. Math. Softw. 29 (2) (2003) 141–164.
[68] A. Frangi, A. Opreni, N. Boni, P. Fedeli, R. Carminati, M. Merli, G. Mendicino, Nonlinear response of PZT-actuated resonant micromirrors, J. Microelectromech. Syst. 29 (6) (2020) 1421–1430.
[69] C. Gazzola, V. Zega, A. Corigliano, P. Lotton, M. Melon, A reduced-order-model-based equivalent circuit for piezoelectric micro-electro-mechanical-system loudspeakers modeling, J. Acoust. Soc. Am. 155 (2) (2024) 1503–1514.